

*Supplementary Information*

## **Oriented Attachment Growth of Monocrystalline Cuprous Oxide Nanowires in Pure Water**

Jun Meng,<sup>a, e</sup> Chengyi Hou,<sup>b, c\*</sup> Hongzhi Wang,<sup>b</sup> Qijin Chi,<sup>c</sup> Yi Gao,<sup>a, d</sup> and Beien Zhu<sup>a, d\*</sup>

- a. Division of Interfacial Water and Key Laboratory of Interfacial Physics and Technology, Shanghai Institute of Applied Physics, Chinese Academy of Sciences, Shanghai 201800, China*
- b. State Key Laboratory for Modification of Chemical Fibers and Polymer Materials, College of Materials Science and Engineering, Donghua University, Shanghai, 201620, People's Republic of China.*
- c. Department of Chemistry, Technical University of Denmark, DK-2800 Kongens Lyngby, Denmark.*
- d. Shanghai Advanced Research Institute, Chinese Academy of Sciences, Shanghai 201210, China*
- e. University of Chinese Academy of Sciences, Beijing 100049, China*

## Contents

**Figure S1.** HRTEM images of the polycrystalline nanowires of  $\text{Cu}_2\text{O}$  synthesized at  $25^\circ\text{C}$ . Images are taken using FEI Tecnai T20 G<sup>2</sup>. Random coalescence of crystals is clearly seen.

**Figure S2.** XPS spectra of  $\text{Cu}_2\text{O}$  nanowires synthesized (a) at  $25^\circ\text{C}$  and (b) at  $90^\circ\text{C}$ .

**Figure S3.** TEM image (a) and corresponding EELS spectra of Cu-L2, 3 (b) and O-K (c) edges measured in  $\text{Cu}_2\text{O}$  nanowires synthesized at  $90^\circ\text{C}$ . The features and positions of Cu-L2, 3 peaks and O-K peak match well with those for cuprous oxide.

**Figure S4.** The initial transient of coalescence of two  $\text{Cu}_2\text{O}$  nanocrystals synthesized at  $90^\circ\text{C}$ .

**Figure S5.** HRTEM images of the monocrystalline nanowires of  $\text{Cu}_2\text{O}$  synthesized at  $90^\circ\text{C}$ . The left panel is taken using FEI Tecnai T20 G<sup>2</sup>. The right panel is taken using FEI Titan E-Cell 80-300 ST TEM. Even the nanowires are damaged more or less by the electron beam irradiation, the fragments as indicated could clearly show the oriented attachment of nanocrystals.

**Figure S6.** Selected TEM images of  $\text{Cu}_2\text{O}$  nanowires synthesized at  $90^\circ\text{C}$ . The dynamic electrophoretic environment causes nondeterminacy in sample location, therefore there is a chance to observe nanowires that are occurring different assembly stages (i.e., preassembled particles, preassembled wires, and well-assembled wires.) in one TEM specimen. Preassembled nanocrystals and discontinuous/short preassembled nanowires, which is obviously assembled from nanocrystals, can be seen in above TEM images. This observation indicates that the long-range ordering nanowires are originated from particle attachment.

**Figure S7.** TEM images and corresponding SAED patterns of (a and b) QDs synthesized after  $\sim 5$  min at  $25^\circ\text{C}$ , (c and d) coalesced QDs synthesized after  $\sim 1$  min at  $90^\circ\text{C}$ , and (e and f) further coalesced QDs synthesized after  $\sim 5$  min at  $90^\circ\text{C}$ . All samples are cubic  $\text{Cu}_2\text{O}$  according to SAED patterns. Atomic planes are partially indicated in the SAED patterns, while others are invisible from corresponding selected area at the applied TEM beam intensity. It is clear that the QDs synthesized at higher temperature tend to coalesce to form larger particles (Visible grain boundaries are indicated by the red arrow in Figure S7c). With longer reaction period, more QDs will coalesce (Figure S7e), orient, and grow into wire-like structures (see Figure 2d-f).

**Figure S8.** TEM images and the corresponding SAED patterns of (a) randomly attached  $\text{Cu}_2\text{O}$  nanoaggregation, (b) polycrystalline nanowires of  $\text{Cu}_2\text{O}$ , and (c) monocrystalline nanowires of  $\text{Cu}_2\text{O}$ .

**Figure S9.** The configurations of  $(3\times 3)$   $\text{Cu}_2\text{O}(100):\text{O}$  surface,  $(3\times 2)$   $\text{Cu}_2\text{O}(110):\text{CuO}$  surface and  $(2\times 2)$   $\text{Cu}_2\text{O}(111):\text{O}$  surface and the stable configurations with water molecule

adsorption. (a) Side and top view of the fully relaxed (3×3) Cu<sub>2</sub>O(100):O surface. (b) Side and top views of the configurations of the configuration with a water molecule adsorbed on the fully relaxed (3×3) Cu<sub>2</sub>O(100):O surface. (c) and (d) present the fully relaxed structure of (3×2) Cu<sub>2</sub>O(110):CuO surface and the stable configuration with a water molecule, top and side views are shown. (e) and (f) are the fully relaxed configurations of (2×2) Cu<sub>2</sub>O(111):O surface and the stable structure with a water molecule adsorbed, top and side views are shown.

**Figure S10.** The stable configurations of a water molecule adsorbed on (a) (1×1) Cu<sub>2</sub>O(100):O surface, (b) (1×1) Cu<sub>2</sub>O(110):CuO surface and (c) (1×1) Cu<sub>2</sub>O(111):O surface.

**Figure S11.** Fitted parameters and curves of the entropy of liquid water. The fitting data are from NIST-JANAF Thermochemical TABLEs ( <http://kinetics.nist.gov/janaf/> ).

**Characterization details.**

**Reference**

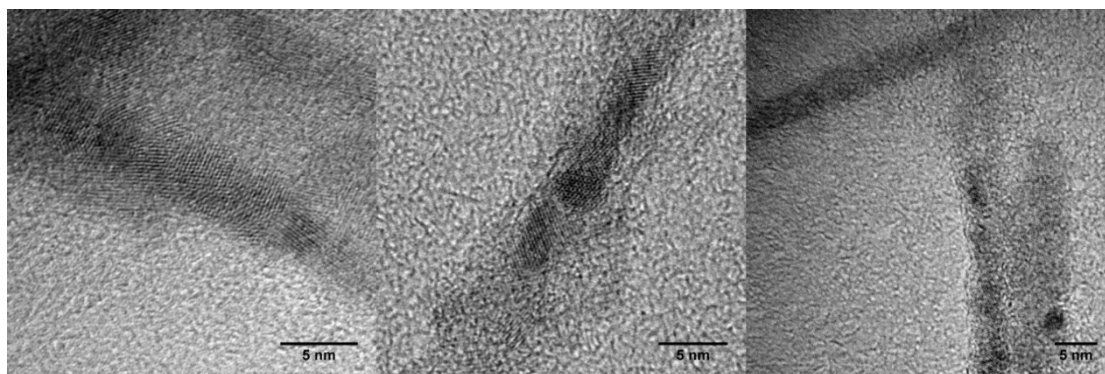


**Figure S1.** HRTEM images of the polycrystalline nanowires of  $\text{Cu}_2\text{O}$  synthesized at  $25^\circ\text{C}$ . Images were taken using FEI Tecnai T20  $G^2$ . Random coalescence of crystals is clearly seen.

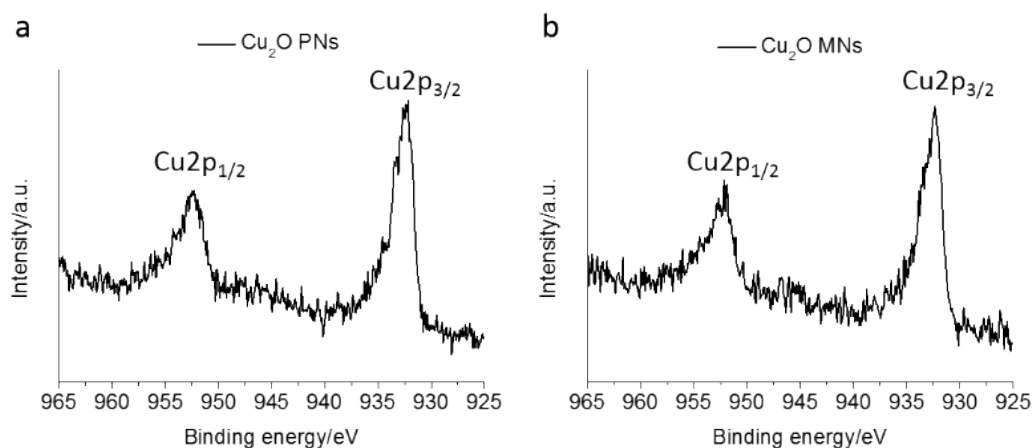


**Figure S2.** XPS spectra of  $\text{Cu}_2\text{O}$  nanowires synthesized (a) at  $25^\circ\text{C}$  and (b) at  $90^\circ\text{C}$ .

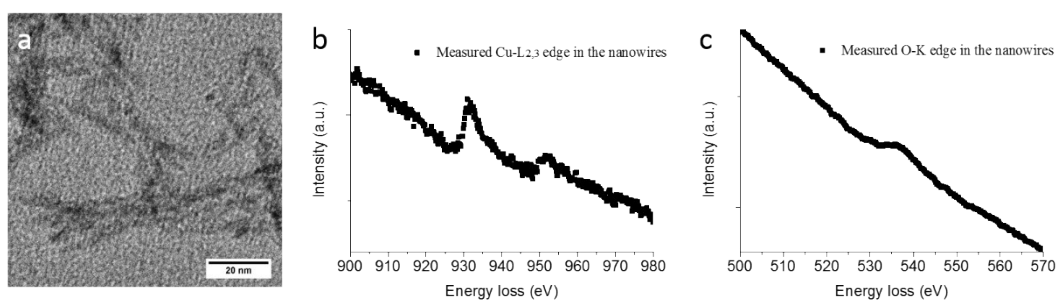


**Figure S3.** TEM image (a) and corresponding EELS spectra of Cu-L2, 3 (b) and O-K (c) edges measured in  $\text{Cu}_2\text{O}$  nanowires synthesized at  $90^\circ\text{C}$ . The features and positions of Cu-L2, 3 peaks and O-K peak match well with those for cuprous oxide.<sup>1</sup>

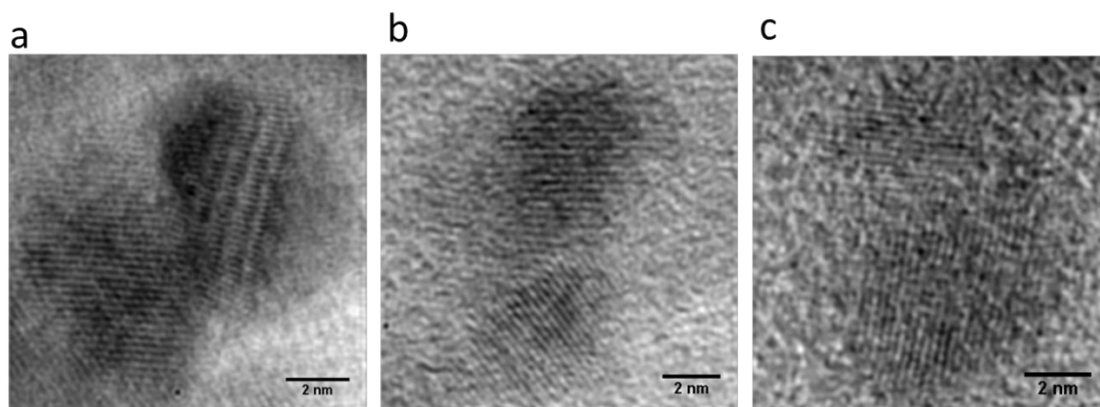


**Figure S4.** The initial transient of coalescence of two  $\text{Cu}_2\text{O}$  nanocrystals synthesized at  $90^\circ\text{C}$ .

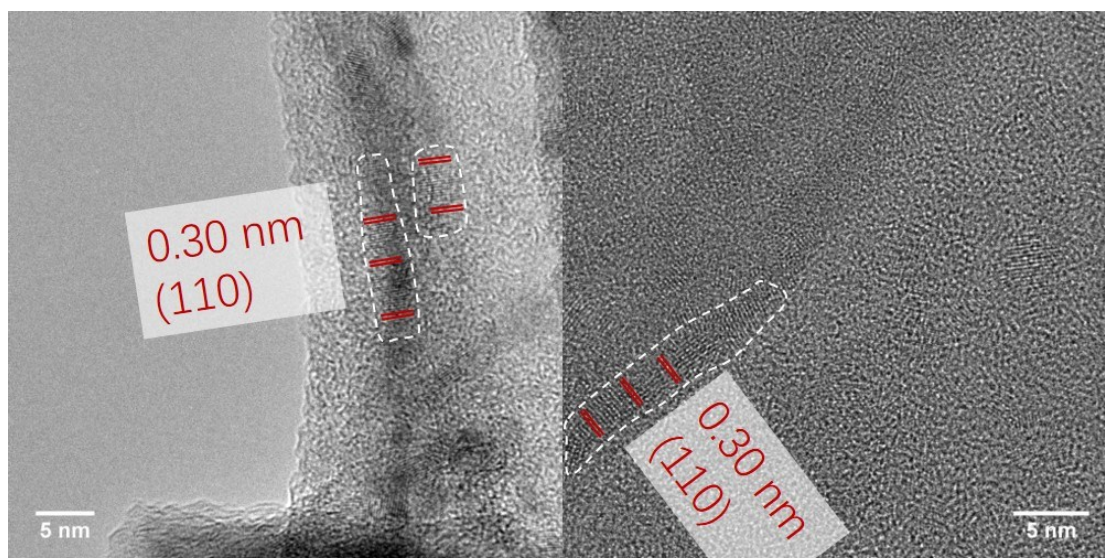


**Figure S5.** HRTEM images of the monocrystalline nanowires of  $\text{Cu}_2\text{O}$  synthesized at  $90^\circ\text{C}$ . The left panel was taken using FEI Tecnai T20 G<sup>2</sup>. The right panel was taken using FEI Titan E-Cell 80-300 ST TEM. Even the nanowires were damaged more or less by the electron beam irradiation, the fragments as indicated could clearly show the oriented attachment of nanocrystals.

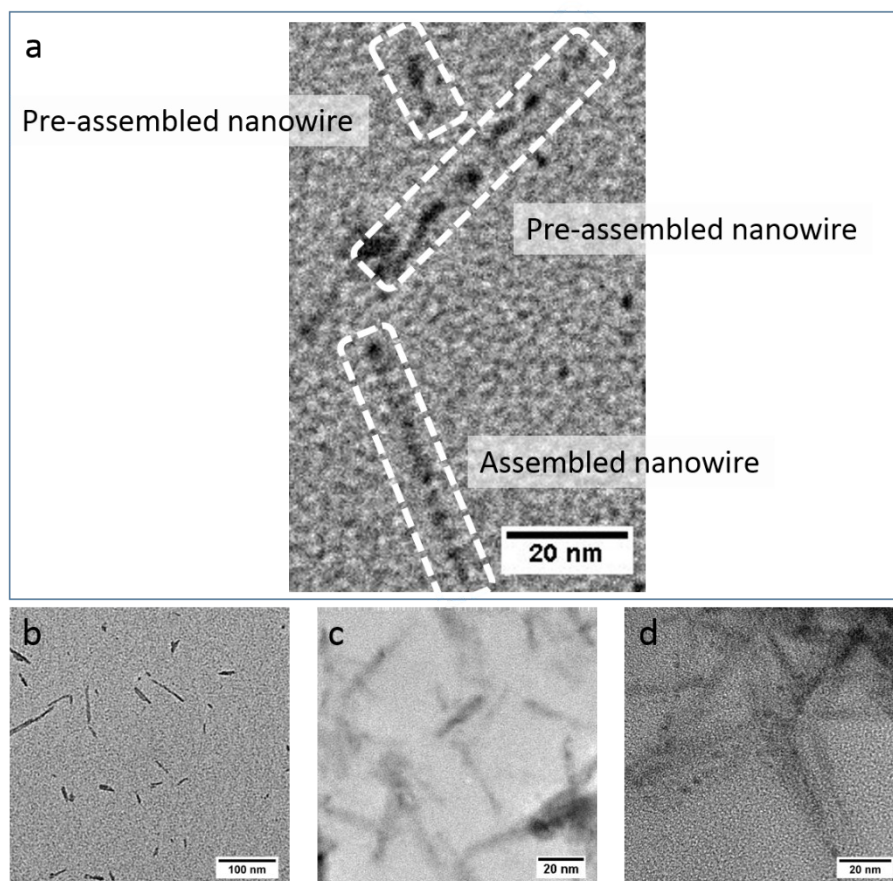


**Figure S6.** Selected TEM images of  $\text{Cu}_2\text{O}$  nanowires synthesized at  $90^\circ\text{C}$ . The dynamic electrophoretic environment causes in sample location, therefore there is a chance to observe nanowires that are occurring different assembly stages (i.e., preassembled particles, preassembled wires, and well-assembled wires.) in one TEM specimen. Preassembled nanocrystals and discontinuous/short preassembled nanowires, which is obviously assembled from nanocrystals, can be seen in above TEM images. This observation indicates that the long-range ordering nanowires form via oriented particle attachment.

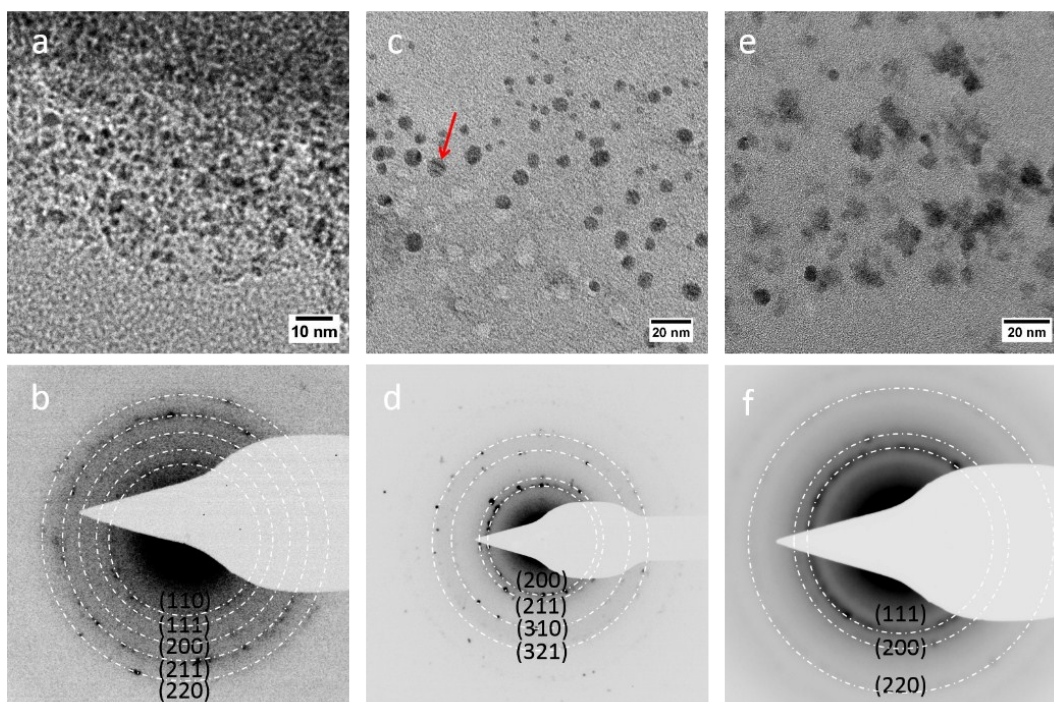


**Figure S7.** TEM images and corresponding SAED patterns of (a and b) QDs synthesized after ~5 min at 25°C, (c and d) coalesced QDs synthesized after ~1 min at 90°C, and (e and f) further coalesced QDs synthesized after ~5 min at 90°C. All samples are cubic Cu<sub>2</sub>O according to SAED patterns. Atomic planes are partially indicated in the SAED patterns, while others are invisible from corresponding selected area at the applied TEM beam intensity. It is clear that the QDs synthesized at higher temperature tend to coalesce to form larger particles (Visible gain boundaries are indicated by the red arrow in Figure S7c). With longer reaction period, more QDs will coalesce (Figure S7e), orient, and grow into wire-like structures (see Figure 2d-f).

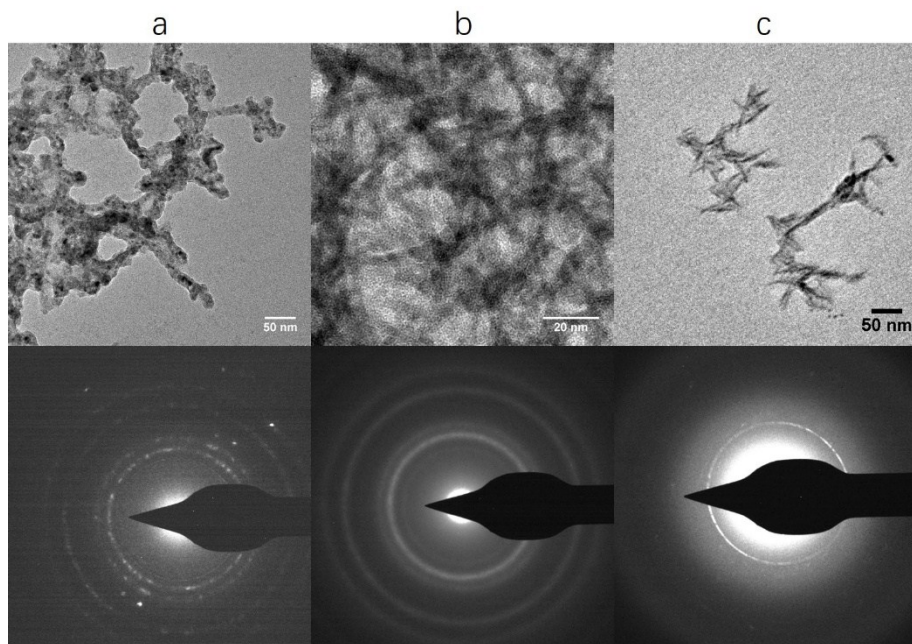


**Figure S8.** TEM images and the corresponding SAED patterns of (a) randomly attached Cu<sub>2</sub>O nanoaggregation, (b) polycrystalline nanowires of Cu<sub>2</sub>O, and (c) monocrystalline nanowires of Cu<sub>2</sub>O. (a) and (b) show clear polycrystalline patterns. In comparison, monocrystalline nanowires of Cu<sub>2</sub>O (c) only shows strong signal from the major plane (110), indicating the oriented attachment growth pattern of Cu<sub>2</sub>O nanowire along the [110] direction, which is in agreement with the results reported in our manuscript. The SAED patterns deliver the crystal structure information of a considerable number of samples, declaring the statistically significance.



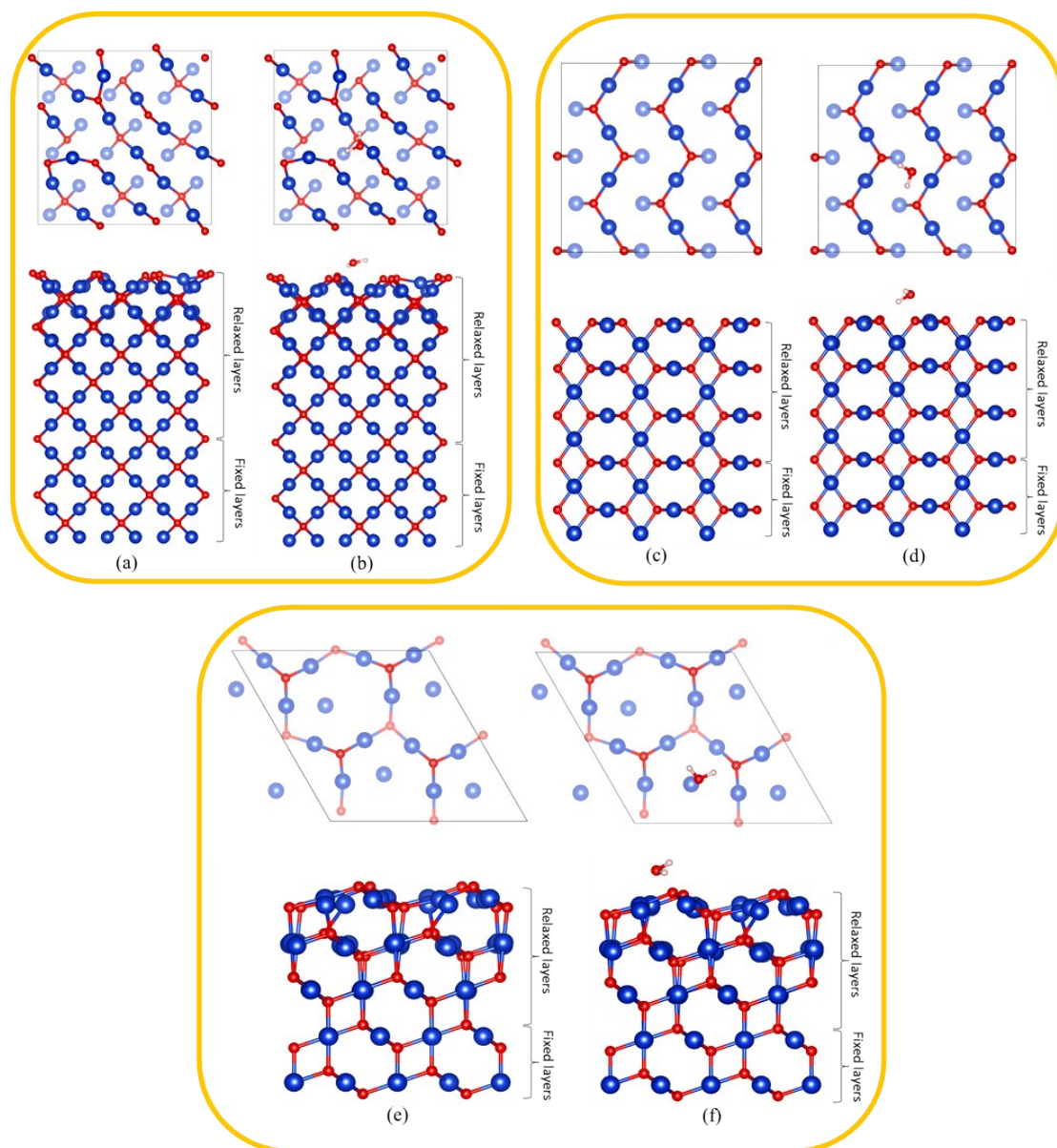


**Figure S9.** The configurations of  $(3 \times 3)$   $\text{Cu}_2\text{O}(100):\text{O}$  surface,  $(3 \times 2)$   $\text{Cu}_2\text{O}(110):\text{CuO}$  surface and  $(2 \times 2)$   $\text{Cu}_2\text{O}(111):\text{O}$  surface and the stable configurations with water molecule adsorption. (a) Side and top view of the fully relaxed  $(3 \times 3)$   $\text{Cu}_2\text{O}(100):\text{O}$  surface. (b) Side and top views of the configurations of the configuration with a water molecule adsorbed on the fully relaxed  $(3 \times 3)$   $\text{Cu}_2\text{O}(100):\text{O}$  surface. (c) and (d) present the fully relaxed structure of  $(3 \times 2)$   $\text{Cu}_2\text{O}(110):\text{CuO}$  surface and the stable configuration with a water molecule, top and side views are shown. (e) and (f) are the fully relaxed configurations of  $(2 \times 2)$   $\text{Cu}_2\text{O}(111):\text{O}$  surface and the stable structure with a water molecule adsorbed, top and side views are shown.

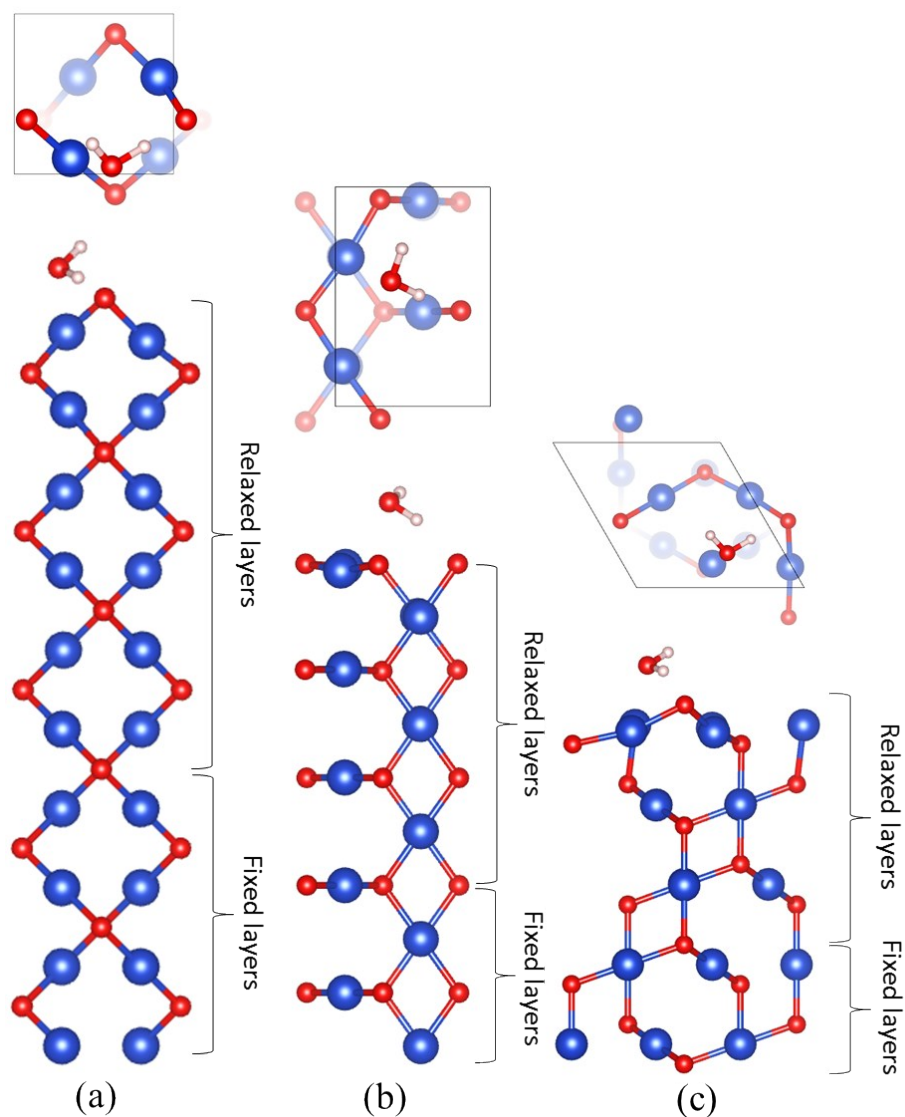


**Figure S10.** The stable configurations of a water molecule adsorbed on (a) (1×1) Cu<sub>2</sub>O(100):O surface, (b) (1×1) Cu<sub>2</sub>O(110):CuO surface and (c) (1×1) Cu<sub>2</sub>O(111):O surface.

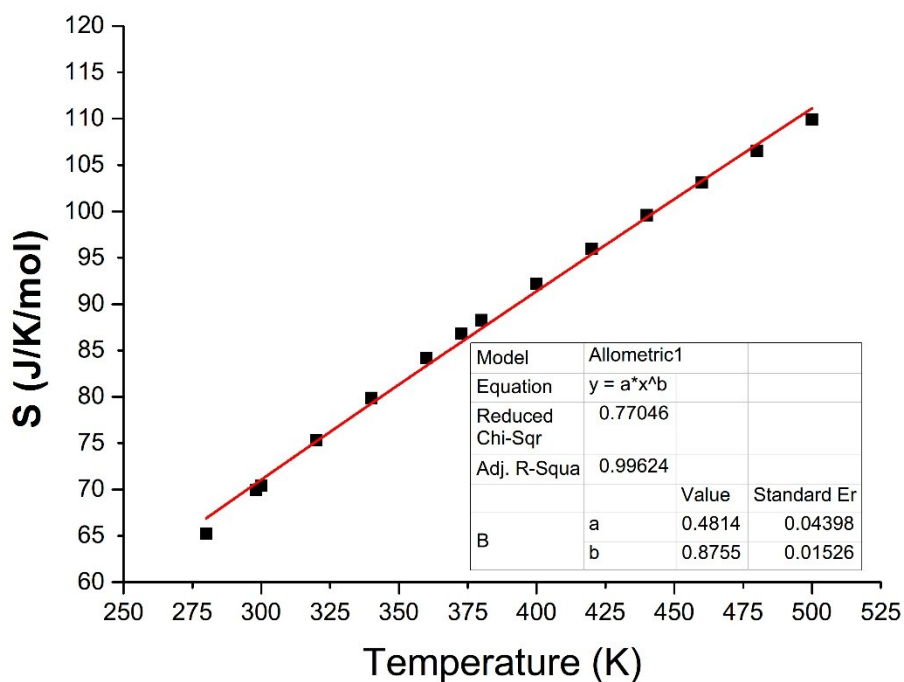


**Figure S11.** Fitted parameters and curves of the entropy of liquid water. The fitting data are from NIST-JANAF Thermochemical TABLES (<http://kinetics.nist.gov/janaf/>).

**Characterizations.** We performed TEM, HRTEM, and EELS on Tecnai G2 T20 and Titan 80-300ST TEMs from FEI Company. Au grids with holey carbon support films were used as support materials for TEM imaging. XPS (Thermo Scientific) was performed to analyze the compositions of samples, with Al-K $\alpha$  (1486 eV) as the excitation X-ray source. Samples were collected from the Milli-Q water solution and dried on Si substrates. The pressure of the analysis chamber was maintained at  $2 \times 10^{-10}$  mbar or lower during measurements.

## Reference

1. C. C. Ahn, O. L. Krivanek, R. P. Burgner, M. M. Disko, P. R. Swann, EELS atlas: a reference guide of electron energy loss spectra covering all stable elements. (Gatan, Warrendale, PA, 1983)